ECS Transactions, 66 (2) 169-176 (2015)
10.1149/06602.0169ecst ©The Electrochemical Society

Study of electrode performance for nanosized $La_{0.4}Sr_{0.6}Co_{0.8}Fe_{0.2}O_{3-\delta}$IT-SOFC cathode

L.V.Mogni[a], K.Yakal-Kremski[b], C.M.Chanquía[a], Z.Gao[b], H.Wang[b], A.Caneiro[a], S.A.Barnett[b]

[a]CONICET, Centro Atómico Bariloche, CNEA. Av. Bustillo 9500, S.C. Bariloche, CP8400 Argentina
[b]Department of Materials Science and Engineering, Northwestern University 2220 Campus Drive, Evanston , IL , 60208 USA

$La_{0.4}Sr_{0.6}Co_{0.8}Fe_{0.2}O_{3-\delta}$ (LSCF4682) perovskite was successfully synthesized by an assisted ammonium nitrate combustion method. The sample shows a sponge-like structure with meso and macro-pores distributed between interconnected nanosized crystallites (~45 nm) with a specific surface area around 8 m^2g^{-1}. Cathode performance of LSCF4682 was investigated in the intermediate temperature range between 400°C-700°C by using symmetrical cell configuration on $La_{0.8}Sr_{0.2}Ga_{0.8}Mg_{0.2}O_{3-\delta}$ (LSGM) electrolyte. The cathode polarization resistances $R_{c,p}$ are 0.067 and 0.035 $\Omega \cdot cm^2$ at 600°C and 700 °C, respectively. The long-term behavior of $R_{c,p}$ was studied by applying an accelerate aging at 800 °C and testing the polarization resistance at 700°C as a function of time. After 500 h of aging, a degradation rate of $\frac{1}{R_{C,P}}\frac{dR_{C,P}}{dt}$ = 0.002 h^{-1}raises the $R_{c,p}$ to 0.1 $\Omega \cdot cm^2$ at 700°C. A maximum power density of 1.23 Wcm^{-2} was achieved at 650 °C testing the LSCF cathode deposited on a porous SLT-LSGM supported multilayer cell. These results demonstrate that this material is a competitive SOFC cathode for the intermediate temperature operation.

Introduction

The main challenge of SOFC technology is to lower the operation temperature range without adversely affecting the overall electrochemical performance. Decreasing the temperature of operation to700°C and below can greatly mitigate the degradation of SOFC components and widens materials selection (i.e. low-cost metallic interconnects), reducing the SOFC stack fabrication and operation costs. As a consequence of the large activation energy, the overall cell losses at intermediate temperature are dominated by cathodic polarization resistance ($R_{C,P}$) (1). Therefore, development of cathode materials with high electrocatalytic activity becomes increasingly critical for the intermediate-temperature SOFC (IT-SOFC). Two complementary strategies have been proposed to enhance the cathode performance: the use of mixed conductor perovskites as cathodes and the incorporation of nanostructured materials through new routes of synthesis.

The $Ba_{0.5}Sr_{0.5}Co_{0.8}Fe_{0.2}O_{3-\delta}$ (BSCF) perovskite was proposed as a potential IT-SOFC cathode (2-3) due to its low $R_{C,P}$. However, its poor structural stability gives rise to a secondary phase, which reduces the performance and compromises the long-term operation

stability of a SOFC built with this cathode. Alternative materials, such as the strontium-lanthanum cobalt-rich perovskites, $La_{1-x}Sr_xCoO_{3-\delta}$ (LSC) and $La_{1-x}Sr_xCo_{1-y}Fe_yO_{3-\delta}$ (LSCF) have also been extensively studied as mixed conductor SOFC cathode materials (4-6). The $R_{C,P}$ of this family of perovskites are higher than that of BSCF, but it is well known that reducing particle size leads to an increase in surface area, thereby reducing the electrode polarization resistance. Thus, different chemical methods have been recently developed to improve the microstructure of LSCF, making them suitable for use as electrodes in IT-SOFC (4, 6-8). However, despite the fact that phase stability is not an issue for LSCF cathodes, other degradation mechanisms cannot be disregarded. One major cause of degradation for Sr-rich perovskites is Sr segregation to the surface, which blocks the O-surface exchange sites (9-10) and decreases the effective surface. However, for nanostructures materials it may be possible that, due to its large surface area, the Sr-segregation would have a minor effect on the long-term degradation. On the other hand, the nanomaterials are liable to suffer from crystallites coarsening, even at the temperatures typical of IT-SOFC operation. The particle coarsening can be a dominant contribution to long-term degradation for nanostructured cathodes, as this leads to reduced surface area (11-12).

In this work, the cathode performance of $La_{0.4}Sr_{0.6}Co_{0.8}Fe_{0.2}O_{3-\delta}$ (LSCF4682)) nanocrystallites was evaluated by $R_{C,P}$ measurements as a function of temperature and time. The overall cell performance of a single cell built with this cathode material was also studied as a function of temperature. The aim of this work was to evaluate whether this material is a competitive SOFC cathodes for the intermediate temperature operation.

Experimental

Synthesis and material characterization

$La_{0.4}Sr_{0.6}Co_{0.8}Fe_{0.2}O_{3-\delta}$ (LSCF4682) powder was synthesized by an assisted ammonium nitrate (NH_4NO_3) combustion method by employing glycine (NH_2CH_2COOH) as fuel and complexing agent. Details of the optimization of the synthesis conditions can be found in (7). Stoichiometric amounts of La_2O_3, $SrCO_3$, metallic Co and Fe were dissolved in a dilute solution of $HNO_3$and kept at T ~80 °C for 24 h. Then, necessary amount of NH_2CH_2COOH and 1 g of NH_4NO_3 were added to the metal-nitrates solution. The obtained solution was transferred to a preheated electric heating case and kept at 180 °C. After ~2 h of heating, the spontaneous combustion of the precursor began and a large amount of gases was released. The as-synthesized nano powder was thermal treatment at 800 °C for 6 h in air-atmosphere with a heating rate of 5 °C min^{-1}. To obtain the pure-phase LSCF4682 nanocrystallites, the optimum ratio of the total valences of the fuel (glycine) and the total valences of the oxidizers (nitrates) was $\varphi = 4$ (7).

The phase purity and crystal structure of the LSCF4682 powders were characterized by X-ray diffraction (XRD) using a PANanalytical Empyrean diffractometer with CuK($\alpha1/\alpha2$) lines, a graphite monochromator and a 3D PIXEL detector. The microstructure and morphology of LSCF perovskites was observed by scanning electron microscopy (SEM) by using a SEM-FEG Nova NANO-SEM 230 and by high resolution transmission electron microscopy (HR-TEM) by using a Philips CM 200 UT microscope equipped with an ultra-twin objective lens.

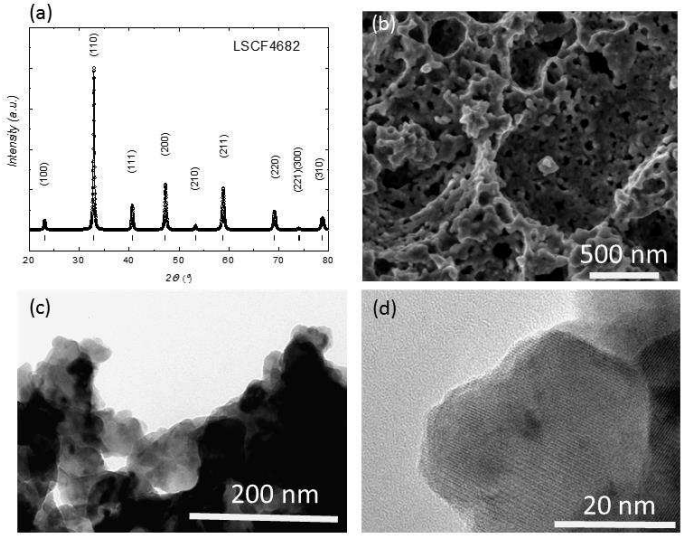

Figure 1. a) XRD pattern, b) SEM and c-d) TEM and HR-TEM images of as synthetized powder of LSCF4682 cathode material.

Electrochemical characterization and long-term operation test

Symmetrical cell fabrication. Symmetrical two-LSCF4682 electrode configuration cells were built on LSGM ($La_{0.8}Sr_{0.2}Ga_{0.8}Mg_{0.2}O_{3-\delta}$, Next Tech Materials Ltd.) electrolytes LSCF4682/LSGM/LSCF4682. Dense LSGM was obtained by uniaxially pressing followed by a sintering treatment at 1500 °C for 6 h. In order to improve the adhesion and to reduce the contact resistance in the electrode/electrolyte interface, a porous layer of LSGM was deposited by spin coating and fired at 1350 °C during 1 h onto both faces of the dense LSGM electrolyte. An ink of LSCF4682 with PVB (polyvinyl butyral), PVP (polyvinylpirrolidone) and α-terpineol, dissolved in isopropyl alcohol was used to deposit the electrodes by spin coating onto both surfaces of the LSGM electrolyte. These symmetrical cells were thermally treated at 800°C (heating rate 7 °C min^{-1}) for 2 h.

Cathode electrochemical characterization as a function of temperature. Surface normalized $R_{C,P}$ was determined from electrochemical impedance spectroscopy (EIS). The symmetrical (LSCF4682/LSGM/LSCF4682) configuration was tested in air as a function of temperature between 400 and 700 °C. The EIS spectra were collected in a frequency range between 10^6 to 0.01 Hz with signal amplitude of 10mV at 0 bias voltage by using a frequency response analyzer (FRA) coupled to an AUTOLAB PGSTAT32.

Cathode electrochemical characterization as a function of time. The time-dependent evolution of $R_{C,P}$ was also studied by EIS. A new symmetrical LSCF4682/LSGM/LSCF4682 cell was prepared and tested as a function of time. In order to reduce the time for data acquisition, the aging of the cathode was accelerated by maintaining the cell at 800 °C during the left time out of the measurement at 700 ºC. The aging tests were run for more than 500 h. The results were compared with that of a commercial $La_{0.6}Sr_{0.4}Co_{0.2}Fe_{0.8}O_{3-\delta}$ cathode (Praxair LSCF6428). The commercial material was aged and EIS-tested at 700 °C.

Cell testing

SOFC tests were performed on single cells of anode–electrolyte–cathode systems. The samples were constructed from a porous $Sr_{0.8}La_{0.2}TiO_{3-\delta}$ SLT-LSGM supported multilayer cell (13). The anode consists of a Ni infiltrated porous LSGM separated from the cathode side by a thin dense LSGM electrolyte. The cathode was prepared as a bilayer electrode consisting of a thin LSGM porous interlayer and a thicker LSCF4682-LSGM 50% composite. The cathode was first deposited by spin coating followed by a heat treatment at 800 °C, similar to the symmetrical cell preparation. The complete cell microstructure was observed by SEM-FEG (Nova NANO-SEM 230).Voltage and power density versus current density were measured as a function of temperature between 500 and 650 °C, flowing 200 sccm of air to the cathode side and 100 sccm humidified H_2 to the anode side.

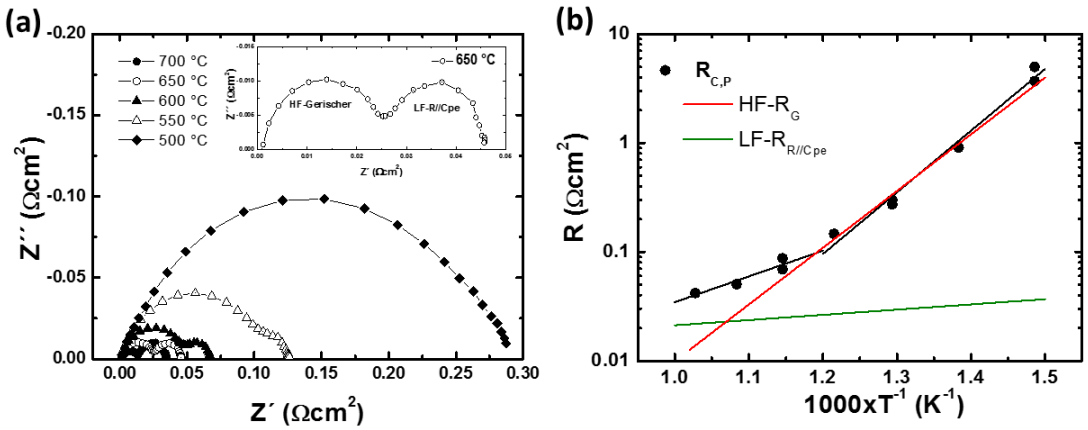

Figure 2. a) EIS spectra collected in air between 500 and 700 °C. b) Arrhenius plot of the cathodic polarization resistance ($R_{C,P}$) and the high and low frequency contributions to the overall $R_{C,P}$.

Discussion

The assisted ammonium nitrate combustion method was previously optimized to obtain pure $La_{0.4}Sr_{0.6}Co_{0.8}Fe_{0.2}O_{3-\delta}$ nanopowders at 800°C (7). Figure 1a shows the XRD pattern of the single phase cubic perovskite obtained. Figures 1 b, c and d, show the microstructure of the as synthetized powder observed by SEM, TEM and HR-TEM. It was previously reported that this material present 45 nm crystallite size with an estimated BET specific surface area of 7.9 m^2g^{-1} and a wide BJH-pore size distribution in the mesoporous region (20-40 nm).

The $R_{C,P}$, determined by EIS in symmetrical LSCF4682/LSGM/LSCF4682 cell configuration, was studied in air as a function of temperature. Figure 2a shows the EIS spectra recorded between 500 and 700 °C (EIS spectra at 400 and 450 °C were not included to improve the clarity of this figure). The inset shows the detail of the spectra collected at 650 °C where two arc can be distinguish. By using the electrical equivalent circuit approximation, a Gerisher type impedance was attributed to the high frequency arc (HF-G) and a resistor-capacitor circuit to the low frequency arc (LF-R//Cpe). A previous study of EIS as a function of O_2 partial pressure proposed a mechanism to describe the cathode reaction (7).Figure 2b shows the Arrhenius-like dependence of the cathodic polarization resistance ($R_{C,P}$) with temperature and the contributions to the overall electrode mechanism

corresponding to the high (HF-R_G) and low (LF-R//Cpe). The unique morphology achieved by the combustion method, which exhibits a specific surface area around 8 m^2g^{-1}, good interconnectivity of grains and a considerable fraction of mesopores induce a change of mechanism controlling the O-surface rate. Below 600 °C, the mechanism of reaction is dominated by the O-surface and transport rates with a high activation energy (See Figure 2b), whereas as T increases the mass transfer due to the O_2 gas diffusion becomes important and the activation energy is reduced (7).

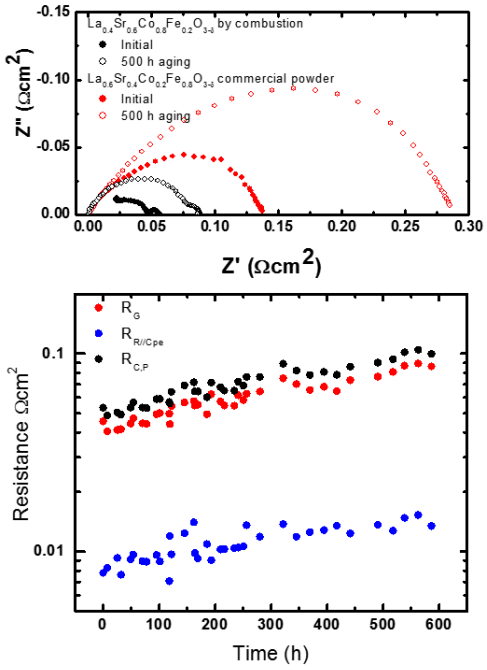

Figure 3. a) Comparison between EIS spectra taken at 700 °C before and after 500 h of aging test carried out at 800 and 700˚C for LSCF4682 and LSCF6482 cathodes, respectively. b) Evolution with time of the polarization resistance of cathode for high (R_G) and low ($R_{R//Cpe}$) frequency contribution to total cathodic polarization resistance($R_{C,P}$).

The time-dependent evolution of the $R_{C,P}$ corresponding to the LSCF4682 powder synthetized by the combustion method, determined by EIS, was compared with that of a LSCF6428 cathode prepared with a commercial powder. For the LSCF4682, the aging of the electrodes were accelerated at 800 °C, with the temperature reduced to 700 °C briefly for the EIS collections. For the commercial cathode, the whole aging test was carried out at 700 °C. Figure 3a shows the initial and 500 h EIS spectra of cells manufactured with either, the commercial LSCF6428 and the LSCF4682 synthetized here.

The degradation rate, defined as $\frac{1}{R_{C,P}}\frac{dR_{C,P}}{dt}$ is considerable lower for the LSCF4682 cathode in comparison with the LSCF6428. Thus, whereas $\frac{1}{R_{C,P}}\frac{dR_{C,P}}{dt} = 0.002\ h^{-1}$ for LSCF4682 aged at 800°C, $\frac{1}{R_{C,P}}\frac{dR_{C,P}}{dt} = 0.006\ h^{-1}$ for LSCF6482 aged at 700°C. Furthermore, after 500 h of aging at 800 °C and more than 100% of $R_{C,P}$increasing, the $R_{C,P}$ of LSCF4682 only raise to 0.1 $\Omega \cdot cm^2$ at 700°C. Figure 3b indicates the time evolution of total cathode

resistance and for both contributions: the HF-G associated to O-surface exchange rate and the LF-R//Cpe related to O_2 gas diffusion. The degradation rate of R_G and $R_{R//Cpe}$ are similar to that of the $R_{C,P}$ suggesting that the origin of degradation is associated to a morphological change with time, affecting both controlling steps of mechanism of cathode reaction, rather than to a chemical change affecting only the surface activity.

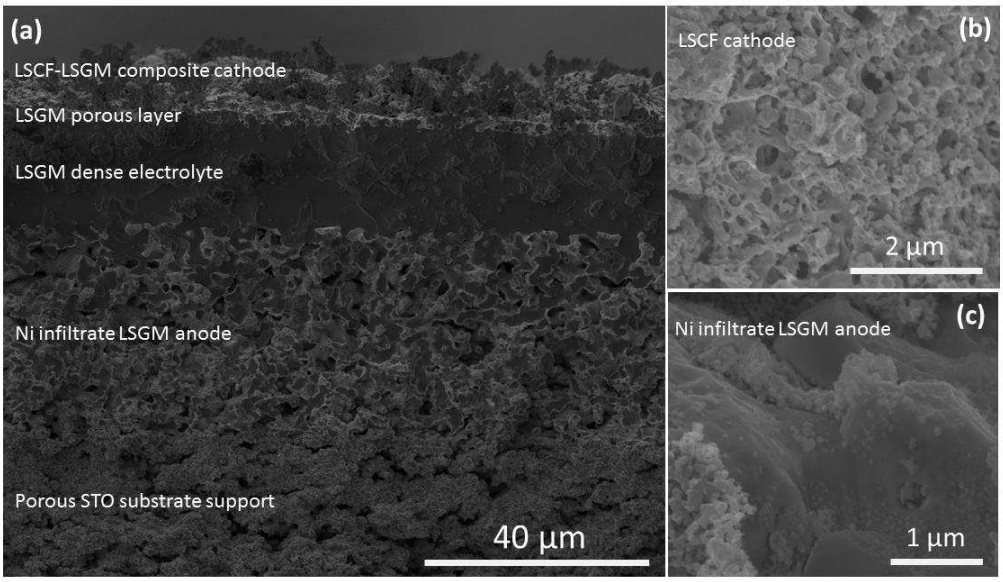

Figure 4. a) SEM cross-section images of SOFC full cell b) cathode consisting of 50 wt. % LSCF4682-LSGM composite c) Ni-LSGM infiltrate anode.

Finally, the LSCF4682 cathode was tested on single cells of anode–electrolyte–cathode systems. Figure 4a shows the microstructure of cross section of the single multilayer cell assembly. The detail of the cathode and Ni-infiltrate anode microstructure is present in Figure 4 b and c, respectively. Figure 5 shows I-V and I-P curves collected between 500 and 650 °C. A maximum power density of 1.23 Wcm^{-2} was achieved at 650 °C. Above 600 °C, the gas mass transfer controls the power density at high current density in agreement with the oxygen reduction mechanisms previously proposed (7). Table 1 compares the results of this work with other promising cathode materials reported in literature. These results in addition to the long-term stability suggest that the $La_{0.4}Sr_{0.6}Co_{0.8}Fe_{0.2}O_{3-\delta}$synthetized by the NH_4NO_3 assisted combustion method is a competitive IT-SOFC cathode.

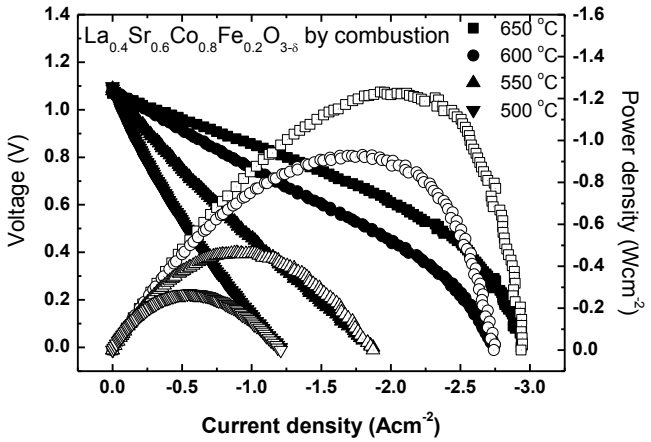

Figure 5. Voltage and power density versus current density measured between 200 sccm of air in cathode side and 100 sccm humidified H_2 in the anode side as a function of temperature.

TABLE I. Comparison between $R_{C,P}$ and maximum power density at 600 °C of LSCF4682 obtained in this work and similar cathode material reported in literature.

Cathode composition	$R_{C,P}$(Ωcm^2)	Power density (Wcm^{-2})	Synthesis method	Ref
$La_{0.4}Sr_{0.6}Co_{0.8}Fe_{0.2}O_{3-\delta}$/LSGM	0.067	0.95	NH_4NO_3 assisted combustion	This work
$La_{0.6}Sr_{0.4}CoO_{3-\delta}$/GDC	0.052	1.58	Pechini	(14)
$La_{0.4}Sr_{0.6}CoO_{3-\delta}$/GDC	0.13	1.34	Pechini	(14)
$La_{0.1}Sr_{0.9}Co_{0.8}Fe_{0.2}O_{3-\delta}$/GDC	0.05	1.3	Solid State Reaction	(15)
$La_{0.6}Sr_{0.4}Co_{0.2}Fe_{0.8}O_{3-\delta}$/LSGM	0.68	0.3	Commercial powder Praxair Inc.	(16)
$Ba_{0.5}Sr_{0.5}Co_{0.8}Fe_{0.2}O_{3-\delta}$/GDC	0.051-0.071	1.01	EDTA-citrate complexing sol–gel	(17)
$Ba_{0.5}Sr_{0.5}Co_{0.8}Fe_{0.2}O_{3-\delta}$/GDC	0.09	0.728	EDTA-citrate complexing sol–gel	(18)
$Sm_{0.5}Sr_{0.5}CoO_{3-\delta}$/SDC	0.1	0.75	Commercial powder Praxair Inc	(19)
$LaBa_{0.5}Sr_{0.5}Co_2O_{6-\delta}$/GDC	0.126	1.254	Pechini	(20)
$PrBa_{0.5}Sr_{0.5}Co_2O_{6-\delta}$/GDC	0.093	1.22	Pechini	(21)
$GdBa_{0.5}Sr_{0.5}Co_2O_{6-\delta}$/GDC	0.123	1.25	Pechini	(22)
$GdBa_{0.5}Sr_{0.5}CoFeO_{6-\delta}$ /GDC	0.067	1.31	Pechini	(22)

GDC: Gadolinium doped ceria; SDC: Samarium doped ceria

Conclusion

$La_{0.4}Sr_{0.6}Co_{0.8}Fe_{0.2}O_{3-\delta}$ perovskite oxides have been synthesized by an NH_4NO_3 assisted glycine combustion method and studied as potential SOFC cathode material for low-temperature operation. The unique morphology displaying specific surface area around 8 m^2g^{-1}, good interconnectivity of nanocrystallites and a considerable volume fraction of mesopores results in a low cathodic polarization resistance ($R_{c,p}$ = 0.067 Ω·cm^2 at 600°C) mainly dominated by O-surface exchange rate and O_2 gas diffusion. This cathode

also exhibits a degradation rate of $\frac{1}{R_{C,P}}\frac{dR_{C,P}}{dt}$ = 0.002 h^{-1} during long-term accelerated aging test at 800 °C and a high maximum power density (1.23 Wcm^{-2}) at 650 °C.

Acknowledgments

The authors at Northwestern University gratefully acknowledge support by theUS Department of Energy Basic Energy Science program (Grant # DE-FG02-05ER46255). The authors at Centro Atomico Bariloche appreciate the financial support of Comision Nacional de EnergiaAtomica (CNEA), Consejo Nacional de Investigaciones Científicas (CONICET), Agencia Nacional de Promoción de Ciencia y Tecnología (AGNPCyT) yUniversidad Nacional de Cuyo. The authors acknowledge to Dr. H. Troiani for his assistance with HR-TEM images. L. Mogni is especially grateful to the Fulbright – CONICET Postdoc Grant Program.

References

1. Steele, B.C.H. and A. Heinzel, *Nature*, **414**(6861) 345-352 (2001).
2. Shao, Z.P. and S.M. Haile, *Nature*, **431**(7005) 170-173 (2004).
3. Zhou, W., R. Ran, and Z. Shao, *J. Power Sources*. **192**(2) 231-246 (2009).
4. Hayd, J., et al. *J. Power Sources*, **196**(17) 7263-7270 (2011)
5. H orita, T., et al.. *Electrochem. Acta,***46**, 1837-1845 (2001).
6. Deganello, F., et al., *J. Electrochem. Soc.***154**(2) A89 (2007).
7. Chanquía, C.M., et al., *J. Power Sources*, **270** 457-467 (2014).
8. Baqué, L., et al., *Electrochem. Comm.*, **10**(12) 1905-1908 (2008).
9. Kubicek, M., et al., *J. Electrochem. Soc.*, **158**(6) B727-B734 (2011).
10. Finsterbusch, M., et al., *Solid State Ionics*, **212** 77-80 (2012).
11. Lu, Y., et al., *J. Electrochem. Soc*., **161**(4) F561-F568 (2014).
12. Shah, M., et al. *Solid State Ionics*, **187**(1) 64-67 (2011).
13. Gao, Z., et al. *Adv. Func. Mat*., **24**(36) 5703-5709 (2014).
14. Gwon, O., et al., *Int.J. Hydrogen Energy*, **39** (35), 20806-20811 (2014).
15. Choi, M.B., et al., *J. Power Sources*, **220** 377-382 (2012).
16. Lin, Y. and S. Barnett, *Solid State Ionics*, **179**(11-12) 420-427 (2008).
17. Zongping Shao, S.M.H., *Nature***431** 170-173, (2004).
18. Zhou, W., et al., *J Power Sources*, **182**(1) 24-31 (2008).
19. Zhang, X., et al., J.Power Sources, **160**(2) 1211-1216 (2006).
20. Choi, S., et al., *Electrochem. Comm*., **34** 5-8 (2013).
21. Park, S., et al., *Electrochimica Acta*, **125** 683-690 (2014).
22. Kim, J., et al., *J. American Ceramic Society*, **97**(2) 651-656 (2014).